A Comparative Study of the Heat Affected Zone (HAZ) Properties of Boron Containing Low Carbon Steels

O. M. AKSELSEN, Ø. GRONG, and P. E. KVAALE

Quantitative information on the HAZ hardenability of two low carbon microalloyed steels containing different boron levels (11 and 26 ppm B) has been obtained on the basis of the weld thermal simulation technique. The extent to which boron affects the HAZ hardenability was found to depend both on the peak temperature and the base plate boron content, in agreement with predictions based on a theoretical model for quench-induced segregation of boron in steel. At the highest boron level (26 ppm B), the hardenability of the grain refined region was approaching that of the grain coarsened one, which resulted in an approximately uniform microstructure within the transformed parts of the HAZ. However, indications are that additions of boron to conventional low carbon microalloyed steels should be restricted to about 10 to 15 ppm B due to the risk of embrittlement in the grain coarsened region at higher boron concentrations.

I. INTRODUCTION

THE role of boron in steel transformation kinetics has been a subject of research for many years. Extensive studies were carried out on boron containing steels during World War II because of the pressing shortage of strategic metals. These early studies revealed that boron in many respects is a unique alloying element by virtue of its powerful effect on the steel hardenability.[1-4] However, due to the imminent risk of embrittlement (arising from precipitation of borocarbides), additions of boron are currently limited to certain grades of low carbon microalloyed steels and quenched and tempered steels where the hardenability is of particular concern.[5]

Despite the fact that boron containing low carbon steels are used to an increasing extent in various welded structures, surprisingly little information is available in the literature regarding the specific effects of boron on the heat affected zone (HAZ) properties.[6] Consequently, the main objective of the present investigation is to provide preliminary data on the HAZ hardenability and toughness of such steels, which in turn can serve as a basis for future research work within this field.

II. MATERIALS AND EXPERIMENTAL PROCEDURE

The chemical composition and mechanical properties of the two boron containing low carbon steels examined are outlined in Tables I and II. It is apparent from the composition data in Table I that the overall chemistry of the two base plates (in the following designated A and B) is reasonably similar, with the exception of the boron content (11 and 26 ppm, respectively). However, there is a marked difference in the inclusion morphology between steels A and B, the latter one containing stringers of manganese sulfide. This gives rise to a low toughness of steel B in the transverse direction as indicated by the Charpy V Notch (CVN) data in Table II. The pertinent variation in the inclusion morphology between the two steels probably reflects a different base plate hot rolling procedure. This assumption is further substantiated by the fact that the ferrite grain size of steel B was found to be significantly coarser than that of steel A (14.7 μm *vs* 6.9 μm).

Assessment of the HAZ transformation behavior was done on the basis of the weld thermal simulation technique. Specifically, this involved determination of the transformation start and end temperatures from (i) numerical derivation of the temperature-time cooling curve of induction heated hollow cylindrical specimens (of 6 mm length, 5 mm o.d., and 3.5 mm i.d.), and (ii) dilatometry measurements on resistance heated CVN specimens. Sufficient experiments were carried out to establish the full CCT diagrams of the grain coarsened region ($T_p \simeq 1350$ °C) as well as the grain refined region ($T_p \simeq 1000$ °C) of the HAZ. It should be noted that the recorded signals for the bainite reaction both include the acicular ferrite and the more predominant ferrite sideplate transformation. Hence, the temperature range of the acicular ferrite transformation is rather uncertain and is therefore only tentatively indicated in the CCT diagrams.

The volume fraction of the various microstructural constituents was calculated from more than 600 points counted at 500 and 1000× in the light microscope, using the following classification system (Figure 1):

- M — lower bainite and martensite.
- SP — ferrite sideplates (*i.e.*, Widmanstätten ferrite and upper bainite), intergranularly or intragranularly nucleated parallel ferrite laths.
- AF — acicular ferrite, intragranularly nucleated separate ferrite needles of a high aspect ratio.
- F — grain boundary ferrite or polygonal ferrite.
- P — pearlite, preferentially in the form of pearlite bands in the grain refined region at relatively slow cooling rates (similar to that observed in parent plates).

The metallographic examination of the synthetic HAZs also included measurements of the prior austenite grain size (the linear intercept technique) and the Vickers hardness (HV_5) of selected specimens.

O. M. AKSELSEN is with SINTEF-Division of Metallurgy, N-7034 Trondheim-NTH, Norway. Ø. GRONG is with The Norwegian Institute of Technology, N-7034 Trondheim-NTH, Norway. P. E. KVAALE, formerly with SINTEF-Division of Metallurgy, is with Statoil, P.O. Box 300, N-4001 Stavanger, Norway.

Manuscript submitted June 10, 1985.

Table I. Steel Composition in Weight Percent (Plate Thickness: 30 mm)

Steel	C	Mn	Si	P	S	Cr	Ni	Cu	Mo	V	Al	Nb	Ti	N	B	O
A	0.11	1.44	0.37	0.009	0.004	0.02	0.15	0.15	0.02	0.04	0.036	0.017	0.004	0.0040	0.0011	0.0024
B	0.13	1.38	0.30	0.013	0.004	0.03	0.18	0.11	0.07	0.04	0.057	0.002	0.003	0.0035	0.0026	0.0025

Table II. Mechanical Properties (Transverse Specimens)

Steel	Yield Strength (MPa)	Tensile Strength (MPa)	Elongation (Pct)	Notch Toughness at −40 °C (J)
A	385	514	32	242
B	330	510	28	35

Impact testing of the thermally cycled CVN specimens was performed at −20 °C. All CVN data reported in the present investigation are the arithmetic mean of two parallel tests. Both steels were assessed in the transverse (T-L) direction (*i.e.*, the notch parallel to the plate rolling direction). In addition, steel B was tested in the longitudinal (L-T) direction (*i.e.*, the notch perpendicular to the plate rolling direction) to account for an expected anisotropy in the HAZ mechanical properties caused by the presence of elongated manganese sulfide stringers in this particular base metal.

For a more detailed description of the experimental procedure, reference is made to the original technical report.[7]

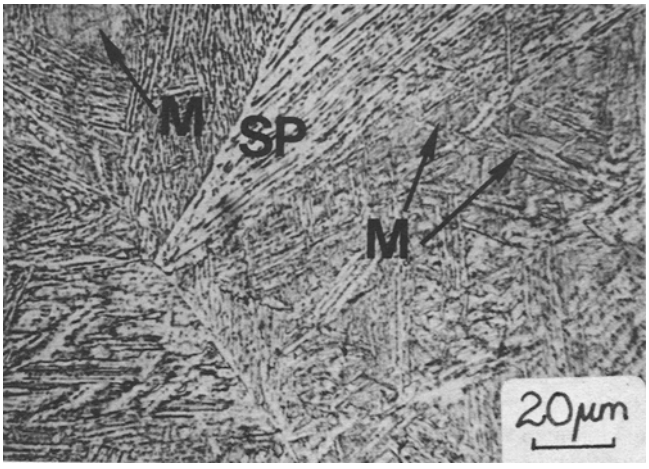

(*a*)

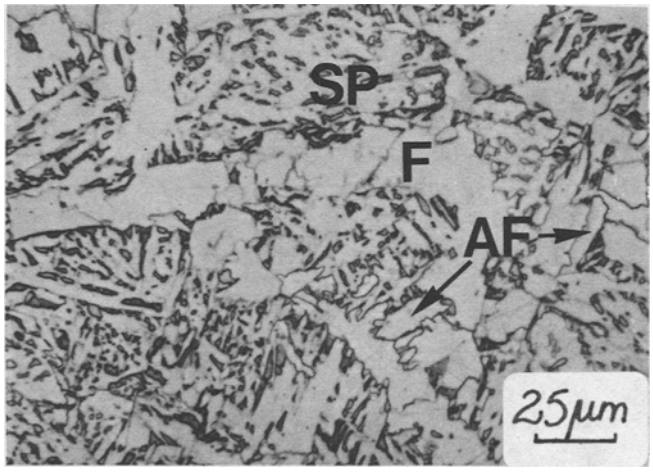

(*b*)

Fig. 1—Classification of HAZ microstructures. The various microconstituents indicated in the figure are defined in the text.

III. RESULTS AND DISCUSSION

A. *HAZ Transformation Behavior*

1. *Steel A (11 ppm B)*

It is apparent from the CCT diagrams contained in Figure 2 that the grain coarsened region ($T_p \simeq 1350$ °C) transforms at a much slower rate than the grain refined one ($T_p \simeq 1000$ °C) for a given cooling time from 800 to 500 °C, $\Delta t_{8/5}$. This finding is not surprising, considering the smaller austenite grain boundary area available for ferrite nucleation in the former case. The microstructures formed within the grain coarsened region consist predominantly of martensite at fast cooling rates ($\Delta t_{8/5}$ less than about 10 seconds) and a mixture of martensite/ferrite sideplates at slower cooling rates (Figure 3(a)). A reduction in the peak temperature from 1350 to 1000 °C resulted in the formation of a duplex microstructure composed of bands of martensite and/or ferrite sideplates in a matrix of polygonal ferrite (Figure 3(b)). The observed difference in the transformation behavior between the grain coarsened and the grain refined region is further evidenced by the hardness data contained in Figure 4.

2. *Steel B (26 ppm B)*

An inspection of the CCT diagrams in Figure 5 reveals a significant effect of boron on the HAZ transformation behavior. At a boron level of 26 ppm B, the hardenability of the grain refined region ($T_p \simeq 1000$ °C) is approaching that of the grain coarsened one, despite the differences in austenite grain size. It is apparent from the micrographs in Figure 6

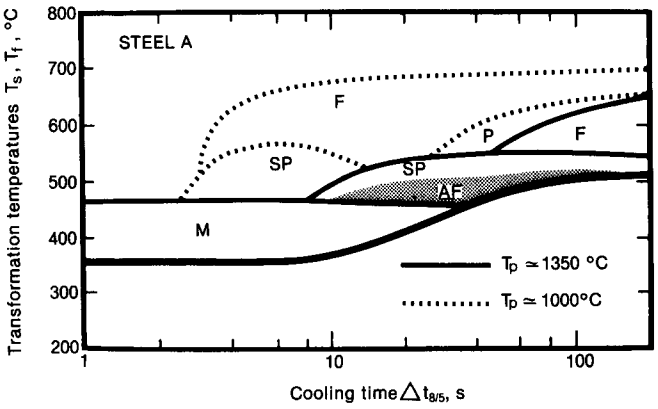

Fig. 2—Steel A—CCT diagram. Solid line: $T_p \simeq 1350$ °C, broken line: $T_p \simeq 1000$ °C.

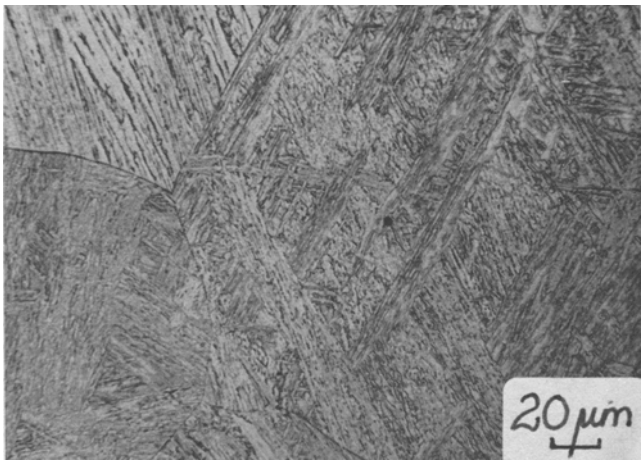

(*a*)

(*b*)

Fig. 3 — Steel A — Typical HAZ microstructures formed within (*a*) the grain coarsened region ($\Delta t_{8/5} \simeq 12$ s), and (*b*) the grain refined region ($\Delta t_{8/5} \simeq 8$ s).

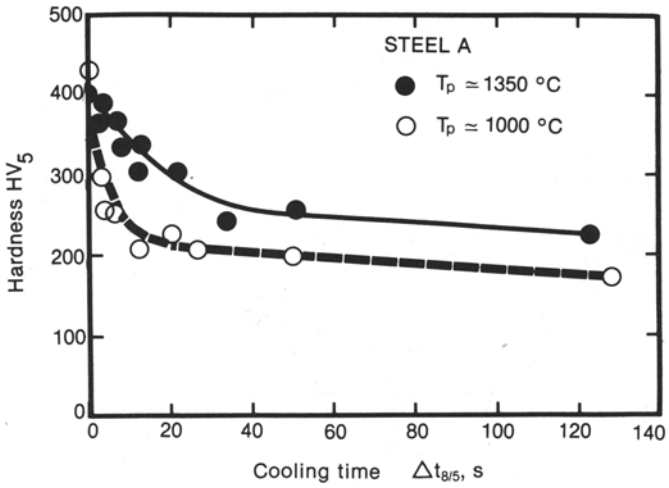

Fig. 4 — Steel A — Effect of $\Delta t_{8/5}$ on the HAZ hardness. Filled symbols: $T_p \simeq 1350$ °C, open symbols: $T_p \simeq 1000$ °C.

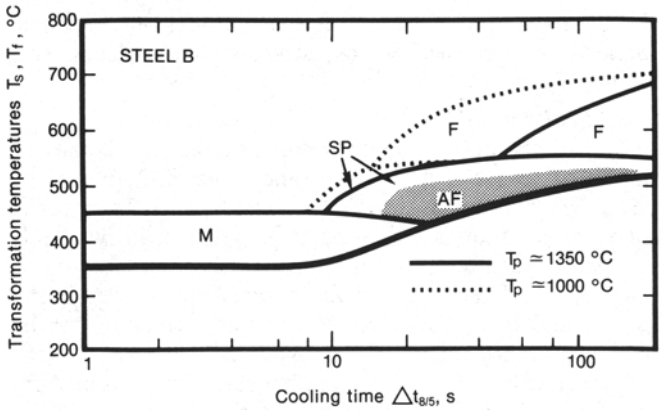

Fig. 5 — Steel B — CCT diagram. Solid line: $T_p \simeq 1350$ °C, broken line: $T_p \simeq 1000$ °C.

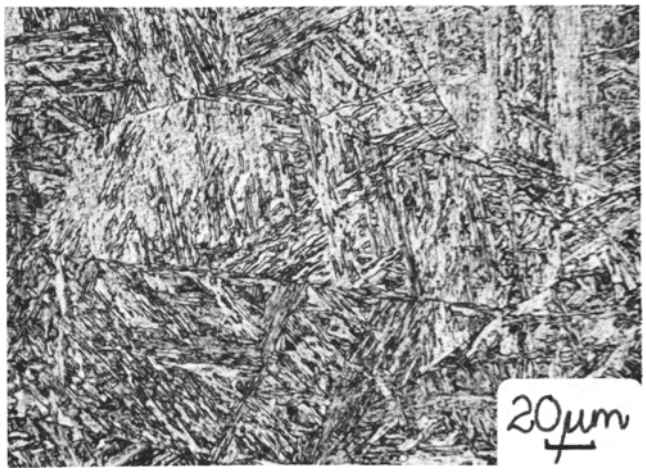

(*a*)

(*b*)

Fig. 6 — Steel B — Typical HAZ microstructures formed within (*a*) the grain coarsened region ($\Delta t_{8/5} = 14$ s), and (*b*) the grain refined region ($\Delta t_{8/5} = 13$ s).

that the fraction of martensite and ferrite sideplates is almost identical in these two regions; so is also the hardness level (Figure 7).

3. *Peak temperature*

The effect of peak temperature on the HAZ hardenability at a constant cooling time from 800 to 500 °C ($\Delta t_{8/5} \simeq 8$ seconds) is shown in Figures 8 and 9. The marked differences in transformation behavior between the two steels are clearly seen both from the microstructure and hardness data contained in the respective figures. At the highest boron level (steel B), a fully martensitic microstructure can be achieved down to about 1050 °C under the cooling conditions employed. This observation is rather surprising and in sharp contrast to the more traditional behavior of steel A, where the fraction of martensite starts to level off at a peak temperature typically below 1200 °C. It should be noted, however, that steel A locally may exhibit high hardness values in the grain refined region (approaching that of steel B) due to the characteristic banded microstructure composed of martensite and ferrite. Since the extent of austenite grain growth occurring during heating at elevated temperatures is approximately the same for both steels (Figure 10), the observed

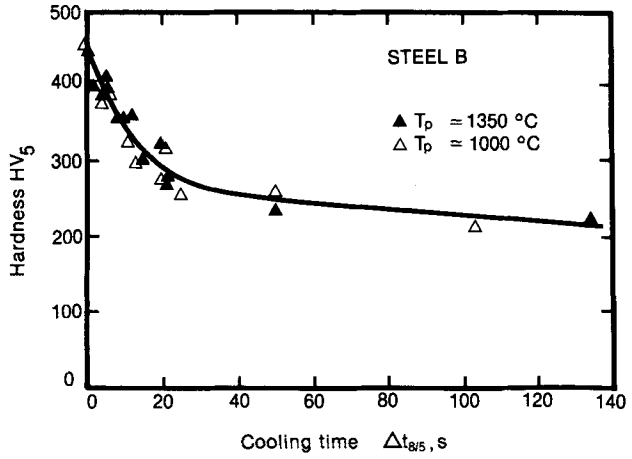

Fig. 7—Steel B—Effect of $\Delta t_{8/5}$ on the HAZ hardness. Filled symbols: $T_p \simeq 1350$ °C, open symbols: $T_p \simeq 1000$ °C.

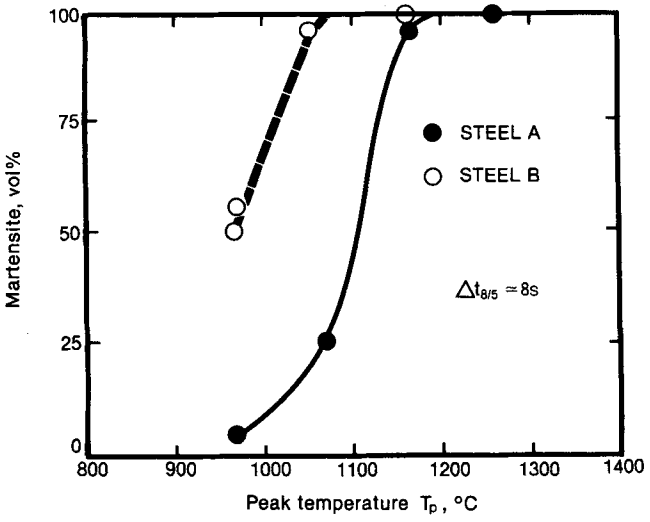

Fig. 8—Effect of peak temperature on the HAZ volume fraction of martensite ($\Delta t_{8/5} \simeq 8$ s). Filled symbols: steel A, open symbols: steel B.

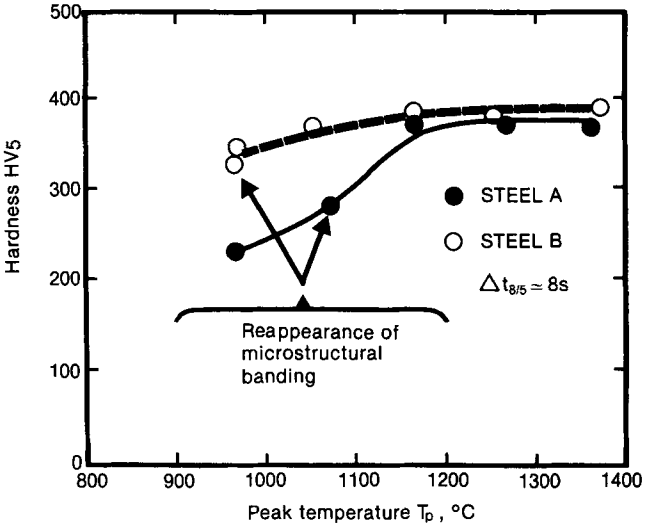

Fig. 9—Effect of peak temperature on the HAZ hardness ($\Delta t_{8/5} \simeq 8$ s). Filled symbols: steel A, open symbols: steel B.

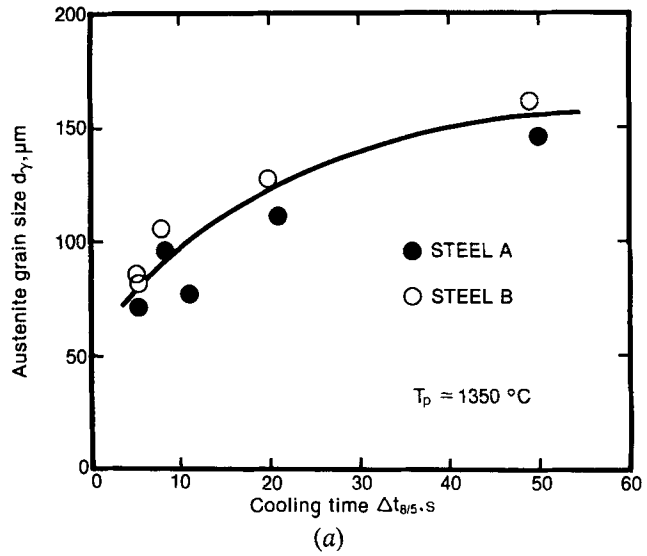

(*a*)

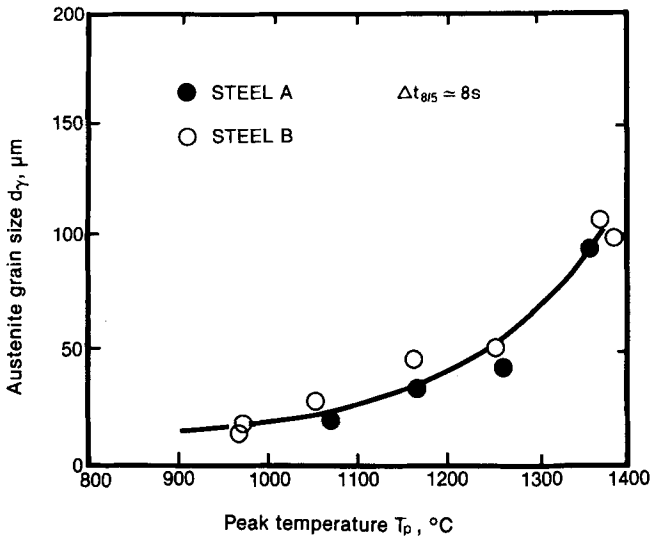

(*b*)

Fig. 10—Influence of weld thermal program on the HAZ austenite grain coarsening behavior. (*a*) Effect of $\Delta t_{8/5}$ ($T_p \simeq 1350$ °C), and (*b*) effect of peak temperature ($\Delta t_{8/5} \simeq 8$ s). Filled symbols: steel A, open symbols: steel B.

differences in hardenability between steels A and B are mainly attributed to the dissimilar boron content.

B. *Impact Testing*

The results from the impact testing of the thermally cycled CVN specimens are shown graphically in Figures 11 and 12. Steel A (Figure 11) reveals satisfactory impact properties in the grain coarsened region over a wide range in $\Delta t_{8/5}$ due to a high fraction of low carbon autotempered martensite. It is interesting to note that the CVN toughness of the grain coarsened region exceeds that of the grain refined one at high and medium cooling rate ($\Delta t_{8/5}$ less than 20 seconds). This situation probably arises from the banded martensite/ferrite microstructure of the latter region.

In the case of steel B (Figure 12), the presence of elongated manganese sulfide stringers, aligned in the plate rolling direction, gives rise to anisotropy in the HAZ impact properties. As expected, a general improvement of the HAZ toughness is observed when testing is performed in the (L-T) direction compared with the (T-L) direction over the entire range of $\Delta t_{8/5}$ examined. A ranking of the two steels (Figure 13) at a constant cooling time from 800 to 500 °C ($\Delta t_{8/5} \simeq 8$ seconds) reveals that the HAZ CVN toughness of steel B in the (L-T) direction is significantly higher than that

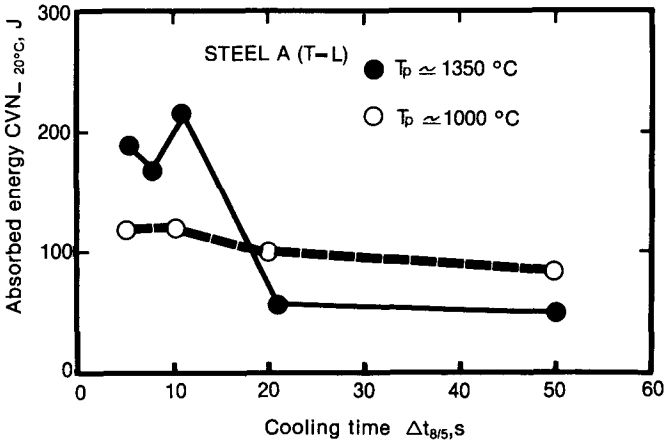

Fig. 11 — Steel A — Effect of $\Delta t_{8/5}$ on the CVN impact energy at −20 °C. Filled symbols: $T_p \simeq 1350$ °C, open symbols: $T_p \simeq 1000$ °C.

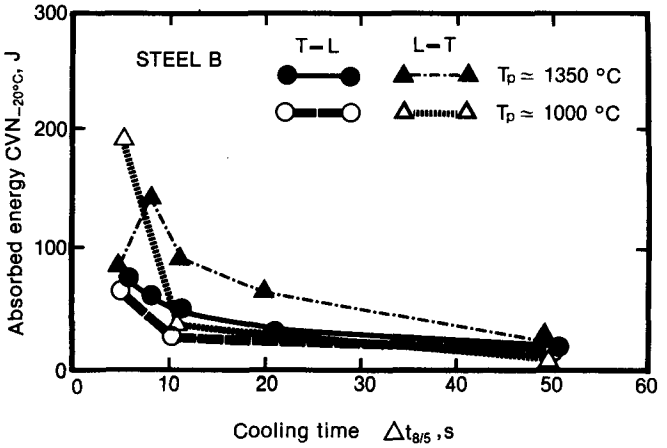

Fig. 12 — Steel B — Effect of $\Delta t_{8/5}$ on the CVN impact energy at −20 °C. Filled symbols: $T_p \simeq 1350$ °C, open symbols: $T_p \simeq 1000$ °C.

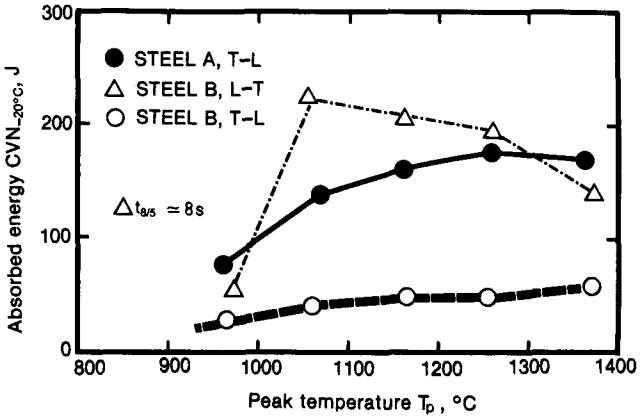

Fig. 13 — Effect of peak temperature on the CVN impact energy at −20 °C ($\Delta t_{8/5} \simeq 8$ s). Filled symbols: steel A, open symbols: steel B.

of steel A within the peak temperature interval from 1000 to 1300 °C. This finding is not surprising, considering the differences in microstructure and notch orientation between the two steels. However, when comparison is made on the basis of the grain coarsened region ($T_p \simeq 1350$ °C), steel A appears to exhibit slightly better impact properties, indicating a possible detrimental effect of boron at high concentrations (to be discussed later).

C. *Boron Hardenability Mechanisms*

The primary effect of boron on the steel hardenability is to raise the energy barrier to ferrite nucleation at the austenite grain boundaries. Although the mechanisms involved are not yet fully understood, free boron is known to segregate extensively to the austenite grain boundaries[8] where it reduces the grain boundary energy.[8,9,10] Based on transformation kinetics theory, it can be rationalized that a decrease in the austenite grain boundary energy will suppress the nucleation of ferrite at these sites.[11] Further enhancement of the energy barrier to ferrite nucleation due to an increase in the total strain energy of the embryo is possible if the free grain boundary volume becomes filled with either boron atoms[1] or borocarbide precipitates, $Fe_{23}(B, C)_6$. In addition, these precipitates have been proposed to inhibit ferrite nucleation at the early stages of transformation by virtue of their semicoherent nature.[12] The inhibition of ferrite nucleation at the coherent side of the austenite grain boundary has been verified experimentally.[13] It should be noted, however, that the effectiveness of boron as a hardenability element is contingent upon an effective protection of boron from nitrogen and oxygen through sufficient additions of titanium and aluminum.

Quantitative information on the extent of boron segregation which occurs to the austenite grain boundaries under various thermal programs can be obtained on the basis of a well established theoretical model for quench-induced segregation of boron in steels.[8,14] At peak temperatures beyond 1000 to 1100 °C, borocarbides and -nitrides present in the base plate will rapidly dissolve in the matrix,[13,15] leading to a significant increase in the amount of free diffusible boron. Generally, solute atoms in a crystal lattice will have an associated strain energy,[8] which implies that it is energetically feasible to pair the solute boron atom with a vacancy. Since the formation of vacancies is a thermally

activated process, it follows that the fraction of boron occupying such sites, $[B]_v$, increases exponentially with temperature:[14]

$$[B]_v = k[B] \exp\left(\frac{-E_f}{RT} + \frac{E_b}{RT}\right) \quad [1]$$

Here k contains various geometric and entropy terms, E_f is the vacancy formation energy, E_b is the vacancy-boron binding energy, and [B] is the bulk concentration of boron.

On introduction of appropriate numbers of k, E_f, and E_b from Williams *et al.*[14] in the case of formation of boron-vacancy complexes in austenite, it follows:

$$[B]_v(\text{ppm}) = 48[B] \exp\left(-\frac{86850}{RT}\right) \quad [2]$$

During cooling, the vacancy concentration initially established at elevated temperatures tends to readjust by elimination of excess point defects at grain boundaries through diffusion. This, in turn, will result in an associated flow of solute boron to the austenite grain boundaries (the extent of which is controlled by the peak temperature and the bulk boron concentration),[14] provided that the diffusivity of the boron-vacancy complexes is higher than that of the vacancies and the boron atoms at all relevant temperatures. The assumption of such highly mobile boron-vacancy complexes is the basis for the theoretical model proposed by Williams *et al.*[14]

Consider now the limiting case where the boron-vacancy complex diffusion to the grain boundaries occurs sufficiently rapid to keep pace with the falling temperature; *i.e.*, the equilibrium concentration, $[B]_v$, is maintained from the peak temperature (T_p) down to the start temperature of the austenite to ferrite transformation (T_s). Viewed against the diffusivity of boron-vacancy complexes in austenite, this is not an unrealistic assumption when the cooling rate is of the order of 50 °C/s (representative of a weld HAZ).[14] Under such conditions, the amount of boron which segregates to the austenite grain boundaries within the temperature interval from T_p to T_s on cooling, $[B]_{gb}$, can approximately be written as:

$$[B]_{gb}(\text{ppm}) = [B]_v^{T_p} - [B]_v^{T_s} \simeq 48[B] \exp\left(-\frac{86850}{RT_p}\right) \quad [3]$$

when $T_p \gg T_s$.

Because the grain boundary area per unit volume (S_v) is inversely proportional to the average austenite grain diameter (d_γ), the product ($d_\gamma [B]_{gb}$) may be taken as a measure of the grain boundary boron concentration. This makes it possible to assess the combined effects of base plate boron content and austenite grain size on the resulting HAZ transformation behavior under various thermal programs. It should be noted that the product ($d_\gamma [B]_{gb}$) does not express the real concentrations of boron at the grain boundaries. Conversion to appropriate units (*e.g.*, atoms per μm^3) requires further assumptions regarding the thickness of the grain boundaries. At the present stage, such refinements are not justified.

In Figure 14 the microstructure data contained in Figure 8 have been replotted *vs* the hardenability parameter ($d_\gamma [B]_{gb}$). Included in Figure 14 are also some results for

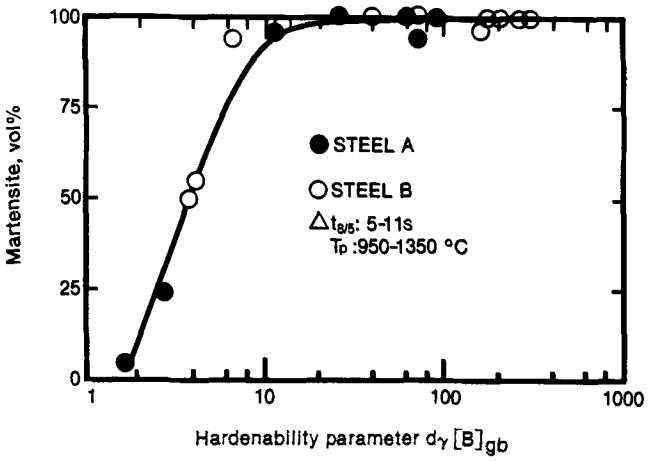

Fig. 14—Correlation between the HAZ volume fraction of martensite and the hardenability parameter ($d_\gamma [B]_{gb}$) ($5\text{ s} \leq \Delta t_{8/5} \leq 11\text{ s}$). Filled symbols: steel A, open symbols: steel B (d_γ in μm, $[B]_{gb}$ in ppm).

$\Delta t_{8/5}$ equal to 5 and 11 seconds to obtain a broader range in the austenite grain size. As it appears from the graph, the data for steels A and B can be represented by one single curve. This result is to be expected if the HAZ transformation behavior for a fixed cooling program is mainly controlled by the grain boundary concentration of boron.

D. *Effect of Boron on the HAZ Toughness*

In Figure 15 the CVN toughness of the synthetic HAZ microstructures outlined in Figure 14 has been replotted *vs* the same hardenability parameter ($d_\gamma [B]_{gb}$). As expected, the best impact properties are achieved for a microstructure consisting primarily of autotempered low carbon martensite. However, the inverted U-shaped curve in the graph reveals a significant drop in the toughness at high ($d_\gamma [B]_{gb}$) values, corresponding to the grain coarsened HAZ of steel B. This situation probably arises from an extensive precipitation of borocarbides, partly at austenite grain boundaries and partly within the matrix as illustrated by the optical micrograph in Figure 16, which clearly will affect the mechanical integrity of the region. Similar observations regarding borocarbide precipitation in the HAZ have also been reported by Devletian[16] for steels of higher carbon contents. It should be

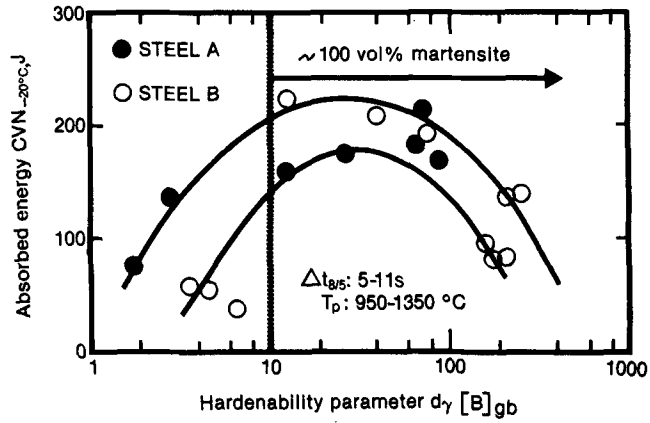

Fig. 15—Correlation between the −20 °C CVN impact energy and the hardenability parameter ($d_\gamma [B]_{gb}$) ($5\text{ s} \leq \Delta t_{8/5} \leq 11\text{ s}$). Filled symbols: steel A (T-L), open symbols: steel B (L-T) (d_γ in μm, $[B]_{gb}$ in ppm).

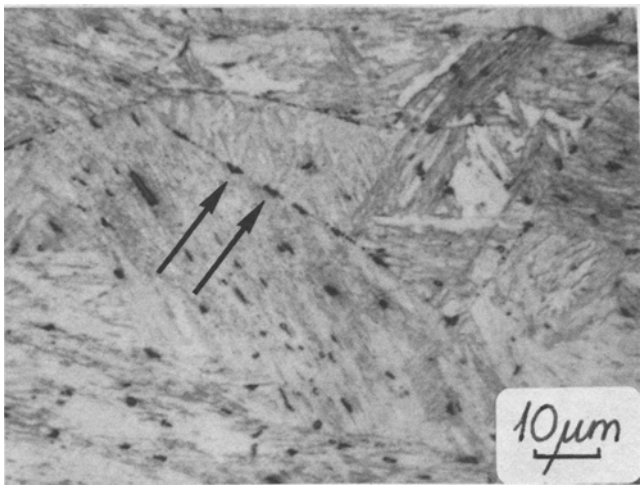

Fig. 16 — Steel B — Precipitation of borocarbides ($T_p \simeq 1350$ °C, $\Delta t_{8/5} \simeq 5$ s). The intergranular precipitates are indicated by arrows in the micrograph.

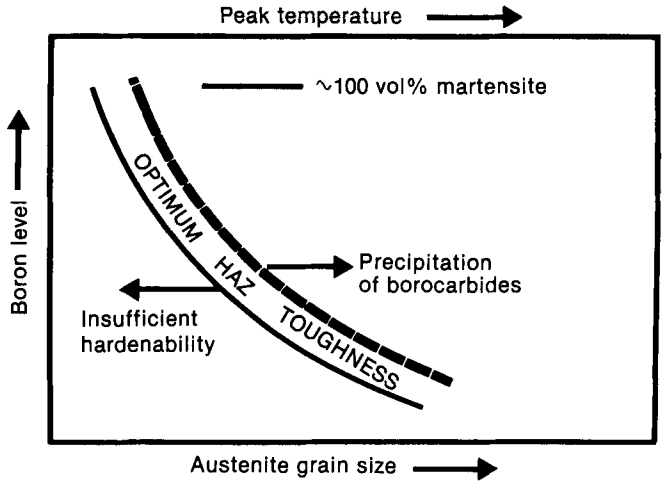

Fig. 18 — Schematic illustration of the combined effects of base plate boron content and austenite grain size (peak temperature) on the HAZ hardenability and resulting impact properties.

noted that the extent of particle precipitation at the austenite grain boundaries in the case of steel B is not sufficient to initiate intergranular fracture as evidenced by the characteristic quasicleavage fracture mode of the grain coarsened region (Figure 17). This leads to the conclusion that the intragranular borocarbides presumably are more detrimental as far as the toughness is concerned.

The CVN data contained in Figure 15 suggest that there exists a critical boron content for a given austenite grain size (peak temperature) which provides optimum HAZ properties from a toughness point of view. With reference to Figure 18, the grain refined region generally exhibits a high tolerance to boron alloying because of a low degree of borocarbide precipitation. In comparison, the grain coarsened region is much more susceptible to this type of embrittlement due to the resulting higher precipitation potential of boron. Thus, the requirement of an adequate HAZ fusion line cleavage resistance finally limits the amount of boron which can be added to the steel for microstructural control.

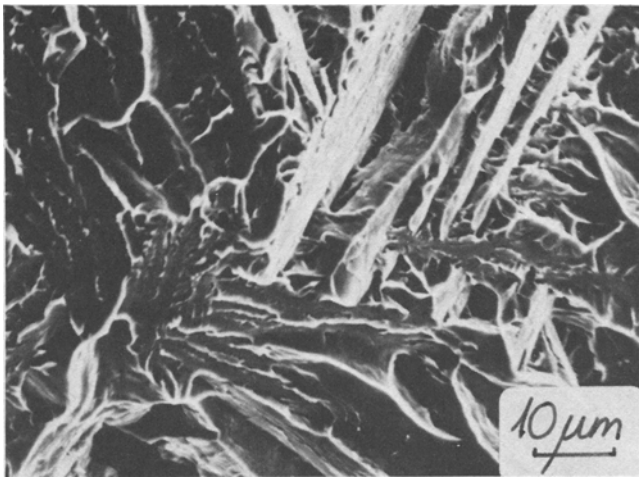

Fig. 17 — Steel B — SEM fractograph of CVN specimen tested at −20 °C ($T_p \simeq 1350$ °C, $\Delta t_{8/5} \simeq 5$ s).

IV. CONCLUSIONS

The basic conclusions that can be drawn from this investigation are as follows:

1. Within the composition range examined (*i.e.*, from 11 to 26 ppm B), boron has only a minor effect on the transformation behavior of the grain coarsened HAZ ($T_p \simeq 1350$ °C).
2. When comparison is made on the basis of the grain refined HAZ ($T_p \simeq 1000$ °C), the hardenability is significantly enhanced by an increase in the base plate boron content. At a boron level of 26 ppm B, the hardenability of the grain refined region is approaching that of the grain coarsened one.
3. The combined effects of base plate boron content and austenite grain size (peak temperature) on the HAZ hardenability can be adequately assessed in terms of a well-established theoretical model for quench-induced segregation of boron in steels.
4. Indications are that additions of boron to conventional low carbon microalloyed steels should be restricted to about 10 to 15 ppm B due to the risk of embrittlement (arising from precipitation of borocarbides) in the grain coarsened HAZ at higher boron concentrations.

ACKNOWLEDGMENTS

The authors appreciate the financial support of STATOIL and the Royal Norwegian Council for Scientific and Industrial Research. In addition, the review and comments by Professor N. Christensen are gratefully acknowledged.

REFERENCES

1. C.R. Simcoe, A.R. Elsea, and G.K. Manning: *J. Metals*, 1955, pp. 193-200.
2. R.A. Grange and J.B. Mitchell: *Trans. ASM*, 1961, vol. 53, pp. 157-85.
3. G.F. Melloy, P.R. Slimmon, and P.P. Podgursky: *Metall. Trans.*, 1973, vol. 4, pp. 2279-89.
4. D.T. Llewellyn and W.T. Cook: *Met. Tech.*, 1974, vol. 1, pp. 517-29.

5. Ø. Grong and O. M. Akselsen: *Met. Constr.*, in press.
6. O. M. Akselsen: Report No. STF34 A84067, SINTEF, Trondheim, August 1984.
7. O. M. Akselsen: Report No. STF34 A84065, SINTEF, Trondheim, June 1984.
8. E. P. Hondros and M. P. Seah: *Physical Metallurgy*, 3rd ed., Elsevier Science Publisher B. V., Amsterdam, 1983, pp. 855-931.
9. J. C. Fisher: *Trans. AIME*, 1954, vol. 200, pp. 1146-47.
10. D. A. Mortimer and M. G. Nicholas: *Met. Sci. J.*, 1976, vol. 10, pp. 326-32.
11. D. A. Porter and K. E. Easterling: *Phase Transformations in Metals and Alloys*, 1st ed., Van Nostrand Reinhold, Wokingham, Berkshire, U.K., 1981, pp. 272-73.
12. R. C. Sharma and G. R. Purdy: *Metall. Trans.*, 1973, vol. 4, pp. 2303-11.
13. Ph. Maitrepierre, D. Thivellier, and R. Tricot: *Metall. Trans. A*, 1975, vol. 5A, pp. 287-301.
14. T. M. Williams, A. M. Stoneham, and D. R. Harris: *Met. Sci. J.*, 1976, vol. 10, pp. 14-19.
15. R. W. Fountain and J. Chipman: *Trans. AIME*, 1962, vol. 224, pp. 599-606.
16. J. H. Devletian: *Weld. J.*, 1976, vol. 55, Res. Suppl., pp. 5s-12s.